Hindawi
Advances in Civil Engineering
Volume 2021, Article ID 4632152, 15 pages
https://doi.org/10.1155/2021/4632152

Research Article

Bayesian Fatigue Life Prediction of Corroded Steel Reinforcing Bars

Wei Wang,[1] Jie Chen,[2] Bo Diao,[3] Xuefei Guan,[4] Jingjing He,[1] and Min Huang[1]

[1]*School of Reliability and Systems Engineering, Beihang University, 37 Xueyuan Rd., Beijing 100191, China*
[2]*Department of Mechanical Engineering, School of Engineering for Matter, Transport and Energy, Arizona State University, Tempe, AZ 85281, USA*
[3]*School of Transportation Science and Engineering, Beihang University, 37 Xueyuan Rd., Beijing 100191, China*
[4]*Graduate School of China Academy of Engineering Physics, Beijing 100193, China*

Correspondence should be addressed to Min Huang; eng.science1@gmail.com

Received 2 July 2021; Revised 15 November 2021; Accepted 2 December 2021; Published 28 December 2021

Academic Editor: Kyriakos Kourousis

This paper presents a general method for fatigue life prediction of corroded steel reinforcing bars. A fatigue testing on standard specimens with pitting corrosion is carried out to obtain corrosion fatigue data. The maximum corrosion degree (MCD), characterizing the most severe site of the corrosion pit, is identified to have a log-linear relationship with the fatigue life. A fatigue life model incorporating the MCD and the stress range for corroded steel reinforcing bars is proposed. The model parameters are identified using the testing data, and the model is considered as the baseline model. To utilize the proposed model for life prediction of corroded steel reinforcing bars with different geometries and working conditions, the Bayesian method is employed to update the baseline model. The effectiveness of the overall method is demonstrated using independent datasets of realistic steel reinforcing bars.

1. Introduction

Fatigue phenomenon in civil engineering is an increasingly prominent concern and cannot be ignored [1–7]. It has been widely reported that the fatigue failure of reinforced concrete (RC) bridge structures is controlled by the failure of steel reinforcing bars [8, 9]; therefore, the fatigue performance of reinforcing bars plays a significant role in the safety of RC structures subjected to cyclic fatigue loading. To make things even worse, in the harsh environment of chloride concentration or relatively severe concrete carbonization, the passive film on reinforcing steel bars is disrupted and the bars are likely to get corroded prematurely over the service life of the RC structures [10–12]. Corrosion can have serious impacts on steel reinforcing bars, including the reduction of the cross-sectional area, passive changes of the mechanical properties (especially for fatigue), and stress concentration near the corrosion pit [11, 13, 14]. Brittle fracture may occur more often and faster for the corroded steel reinforcing bars subjected to fatigue loading compared to the uncorroded bars.

Studies of fatigue behavior of corroded reinforcing bars have been carried out over the past few decades. Fernandez et al. [13] performed a series of fatigue tests consisting of 140 corroded reinforcing bars under 3 stress ranges and reported a negative exponential model correlating the fatigue life with the corrosion degree, which is defined as the ratio between the mass loss and the initial mass. Tang et al. [15] conducted an experimental study on 22 deformed reinforcing bars with corrosion degrees (mass loss ratio) of 0%, 5%, 10%, and 20%. In the study, corrosion damages were made using the impressed current technique, and fatigue life data with different corrosion degrees were analyzed. Li et al. [16] studied the performance of tensile fatigue using 15 plane steel bars with naturally carbonation-induced corrosions. Corrosion degrees ranging from 15% to 30% under 3 stress ranges were used. Results showed that fatigue life of steel reinforcement with natural corrosions has a power law

dependence with the corrosion degree, and the log-scale slope parameter increases with the increasing of the stress range. Ma et al. [17] created semielliptical and triangular corrosion pits on reinforcing bars by removing materials directly. Fatigue life data of the steel reinforcing bars with different notch shapes and sizes were presented. Zhang et al. [18] obtained the fatigue lives of both artificially and naturally corroded reinforcing bars and found that the artificially corroded reinforcing bars are more susceptible to corrosion damage. An empirical fatigue life prediction model was proposed to incorporate the combined influence of the corrosion degree and the stress range.

Although a great deal of efforts has been made in fatigue life prediction of corroded steel reinforcing bars, there still remain challenges for practical engineering applications. In particular, most of the reported fatigue life prediction models are specific to certain circumstances and applications. For instance, model parameters need calibrations when the geometry of the bars or the working condition changes significantly. This is due to the uncertain nature of the corrosion process and the variation of the environment. In addition, the mass loss ratio, which is widely used in those models, characterizes an average influence of the corrosion pit to the fatigue life. It rarely accounts for the most severe location of a corrosion pit. It has been shown that the minimum cross section of a local corrosion pit is the most critical site for fatigue crack initiation, propagation, and final fracture due to stress concentration and cyclic fatigue loads [19–21]. As a result, the average treatment can introduce additional uncertainty into fatigue life prediction. Therefore, a more general fatigue life model taking the local geometry of the corrosion pit into account is highly needed for a reliable life prediction of corroded reinforcing bars.

This study presents a general method for fatigue life prediction of corroded reinforcing bars. To overcome the potential limit of the mass loss ratio parameter, a new parameter defined based on the cross-sectional area reduction is used. To resolve the issue that a model tunned with one set of testing data can yield inaccurate results when it is directly applied to applications with different geometry and working conditions, Bayesian method is used to update the initial baseline model with the observed data specific to the application. The rest of the study is structured as follows. First, experimental work on standard reinforcing steel specimens with pitting corrosion is introduced, and fatigue life testing data are obtained. Next, a regression model is proposed to associate the stress range and the maximum corrosion degree (MCD) with the fatigue life. Following that, Bayesian updating is employed to update the initial baseline model for more general applications, and the effectiveness of the proposed method is demonstrated using data of realistic corroded reinforcing bars. Finally, conclusions are drawn based on the current study.

2. Fatigue Testing of Corroded Specimens

The overall method development process is illustrated in Figure 1. Experimental testing is designed and performed on 14 precorroded standard specimens of steel reinforcements to investigate the corrosion fatigue life under different stress ranges. Two variables, the stress range and the MCD defined as the maximum reduction of the cross-sectional area, are identified as the characterizing factors of the fatigue life. A baseline fatigue life prediction model is proposed by incorporating the two variables. To account for uncertainties from different usage conditions, the Bayesian method is employed to update the baseline model allowing for more general applications. An independent dataset is used for Bayesian updating and method verification.

2.1. Materials and Specimens. A total number of 14 corroded standard specimens made from steel reinforcing bars are prepared, and the fatigue testing data are acquired to build the baseline model. Artificial corrosion pits are developed using the impressed current technique in the NaCl solution. The maximum corrosion degree is measured with the three-dimensional (3D) scan technique. Following this, the axial fatigue testing is carried out under three different stress ranges, and the results of fatigue life are acquired. The degree of corrosions in this study is tentatively controlled to be in the range between 10% and 40% in terms of the maximum cross-sectional area reduction to represent the actual degree of corrosions in practice. Three levels of applied loads are considered to simulate the nominal and overload conditions.

The dimension and an actual specimen used in this study are shown in Figure 2. The specimen is prepared by removing the surface layer of hot-rolled ribbed steel bars (HRB400) with an initial diameter of 20 mm. The chemical composition of the material is shown in Table 1. The geometry and dimension of the final specimens follow the code requirement for both statistic [22] and fatigue testing [23]. The elastic modulus and yield strength of the four uncorroded specimens are shown in Table 2. The mean values of the mechanical properties are calculated and are used as references for fatigue testing.

2.2. Precorrosion and 3D Measurement. The corrosion pit is developed on each of the 14 specimens using an accelerated corrosion process in the solution of 5% NaCl with a current density of 0.6 mA/cm^2. Before corrosion, the specimen is wrapped using watertight insulation tapes to protect the surface from the solution. An elliptical shape of the tape is removed at the location for corrosion damage to expose the metal surface to the solution, as shown in Figure 3(a). Both ends of the specimen are sealed by hot-melt adhesive with one end connected with a wire. A direct-current power supply is used for the corrosion process during which the specimen serves as anode and a separate stainless-steel bar as the cathode, as shown in Figure 3(b). After the corrosion process, the specimen is cleaned and stored in a dry condition for fatigue testing.

Due to the nonuniform corrosion process, the width and depth of the corrosion pit vary along the axial direction. Consequently, the cross-sectional area also varies along the axial direction. The concept of maximum corrosion degree (MCD), $\eta_{\max}$, is proposed to characterize the most severe condition of the corrosion pit and is defined as follows:

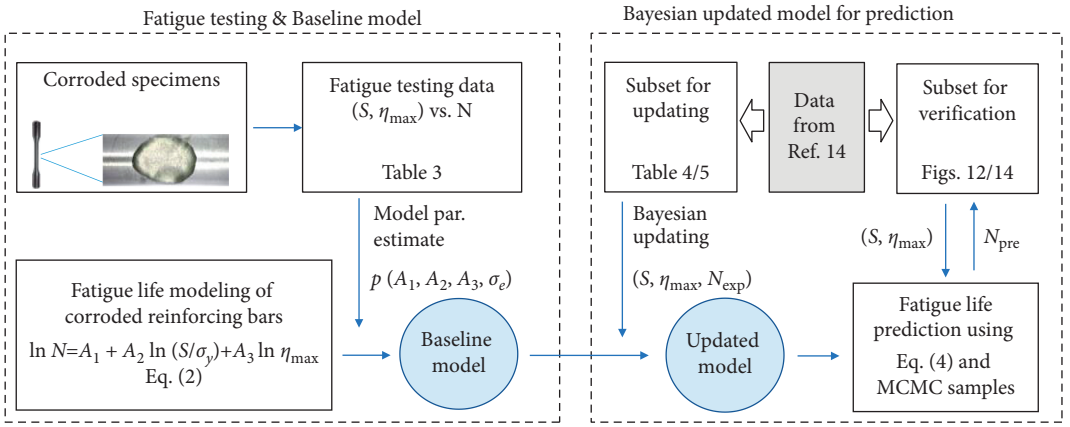

Figure 1: Overall method development process.

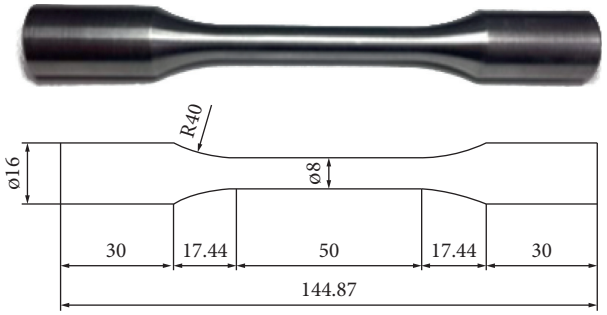

Figure 2: An actual specimen and its dimension (unit: mm).

Table 1: Chemical composition of HRB400 bars.

Chemical composition	C	Si	Mn	P	S	V
Percentage	0.22	0.45	1.34	0.028	0.031	0.033

Table 2: Mechanical properties of HRB400 bars.

Specimen no.	$M1$	$M2$	$M3$	$M4$	Mean value
Elastic modulus E (MPa)	210330	212698	201833	205854	207679
Yielding strength σ_y (MPa)	460.29	463.88	446.09	450.23	455.12

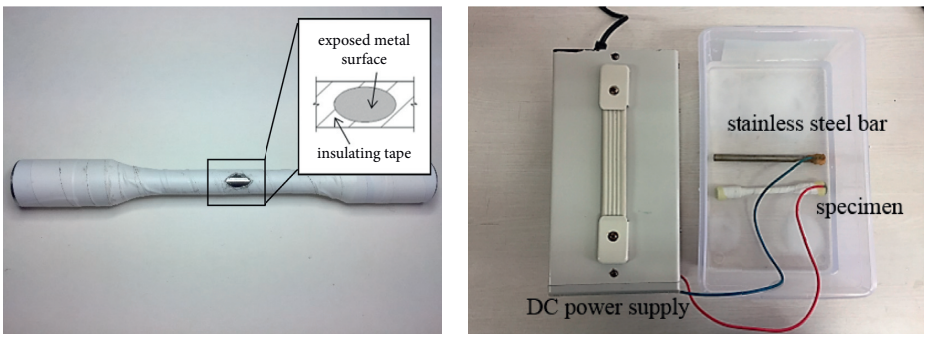

(a) (b)

Figure 3: Treatment of specimen and precorrosion setup. (a) Treatment of specimen before corrosion process. (b) Corrosion environment setup.

$$\eta_{\max} = \frac{1 - A_{\min}}{A_0}, \quad (1)$$

where $A_{\min}$ is the minimum cross-sectional area of the corrosion pit and A_0 is the initial uncorroded cross-sectional area.

A high-resolution 3D laser scanner is used to acquire the surface data of the specimens [24]. The laser scanner can produce a point cloud of the surface. The raw data are processed using the Geomagic wrap software to reconstruct a 3D surface for digital measurement [25]. The reconstructed 3D surface model is imported into the Pro/Engineer software environment to form a solid volume for cross-sectional measurement [26]. The cross-sectional slices are sampled from the solid volume at an interval of 0.1 mm along the axial direction in the corroded region. The areas of the cross-sectional slices are automatically computed in the Pro/Engineering software. The minimum cross-sectional area is identified as $A_{\min}$. One of the specimens (FC3) is used for illustration. The actual corrosion pit of the specimen is shown in Figure 4(a), and the reconstructed 3D surface model is shown in Figure 4(b). The model shown in Figure 4(b) is imported into Pro/Engineer and the minimal cross section in terms of MCD is identified, as shown in Figure 5. The whole digital processing and measurement process is performed for each of the specimens, and the results of MCD are listed in Table 3.

2.3. Fatigue Testing Results and Discussion. The uniaxial fatigue testing is carried out in air condition at room temperature using a sinusoidal load with a stress ratio of 0.1. An electrohydraulic fatigue testing machine (Instron 8801, 100 kN) is used to apply cyclic loads as shown in Figure 6. The loading frequency of the fatigue testing can be configured using the control software. The maximum loading frequency of the electrohydraulic machine is 20 Hz. The maximum frequency is used to reduce the testing time. Based on the testing results of the mechanical properties, the material has a mean yield strength of 455.12 MPa. Three maximum nominal stress levels are chosen as $0.5\sigma_y$, $0.7\sigma_y$, and $0.8\sigma_y$. The stress levels are chosen to represent the normal service load and two overload conditions [27]. Given the stress ratio of 0.1, the corresponding nominal stress ranges are $0.45\sigma_y$, $0.63\sigma_y$, and $0.72\sigma_y$, respectively. The fatigue testing can adopt two loading schemes, namely, the force-controlled (ASTM E466) and the displacement-controlled (ASTM E606). Depending on the context, they are also called stress-controlled or strain-controlled, respectively. For low-cycle fatigue problems where significant plastic strains are involved and the resulting fatigue life is not larger than 10^5 [5], the displacement (strain)-controlled testing scheme is usually used. For high-cycle fatigue where the total strain is elastic strain dominant, the force (stress)-controlled testing scheme is suitable. In this study, the maximum loading force is $0.8\sigma_y$; therefore, the force-controlled testing scheme is employed. The stress ratio and the minimum stress remain constant during the testing process. The nominal stress range is defined as the $(F_{\max} - F_{\min})/A_0$. Terms $F_{\max}$ and $F_{\min}$ are the maximum and the minimum forces, respectively, and A_0 is the uncorroded cross-sectional area. The fatigue testing stops when the specimen is completely fractured and the number of applied load cycles at rupture is recorded as the fatigue life. The applied loads in terms of the normal stress ranges and the actual stress ranges at the MCD cross section for each of the specimens and the associated fatigue life results are shown in Table 3. All the specimens ruptured at their MCD cross sections due to the maximum local stress at the cross section.

Based on the testing results, it can be seen that the fatigue life in general decreases as the actual stress range increases. The observation is consistent with the usual fatigue testing results. The minimal and maximum values of actual stress range in this case are 247.0 MPa and 430 MPa, respectively, which correspond to the largest and smallest fatigue lives of 4060752 and 27611 cycles, respectively. Due to the uncertain corroded surface conditions and the shapes of the MCD, the fatigue life results exhibit the inherent interspecimen uncertainty. For example, there is a noticeable difference in fatigue life between FC7 and FC8 although the actual stress ranges of the two specimens are almost identical.

3. Model Development

3.1. Fatigue Life Prediction Model. The fatigue testing results show that both the stress range and MCD have significant influences on the fatigue life, and they are considered as model independent variables. It is known that the same stress range has different effects on different materials; therefore, the normalized stress range, S/σ_y, is used for model development. The normalized stress range is defined as the ratio between nominal stress range and the yielding stress of the material. Unless stated otherwise, the stress range in the text hereafter refers to the normalized nominal stress range. To identify the relationship between the fatigue life and MCD at different stress ranges, fatigue life versus MCD are presented in Figure 7. A log-linear relationship between the fatigue life and the MCD can be observed under different stress ranges. At the same level of MCD, the fatigue life decreases as the stress range increases.

In view of aforementioned features, a fatigue life model incorporating the combined influence of stress range and MCD is proposed as follows:

$$\ln N = A_1 + A_2 \ln\left(\frac{S}{\sigma_y}\right) + A_3 \ln \eta_{\max}, \quad (2)$$

where N is fatigue life and A_1, A_2, and A_3 are model parameters. It is noteworthy that other forms of regression models can also be adopted. For example, an interaction term $\ln(S/\sigma_y)\ln\eta_{\max}$ can be appended to the right-hand side of equation (2) if it can be justified. The formal and rigorous method for model selection is beyond the scope of this study and can be referred to in other studies [28].

3.2. Probabilistic Parameter Identification. The parameters A_1, A_2, and A_3 of the model equation (2) can be obtained using experimental data. For the deterministic estimation,

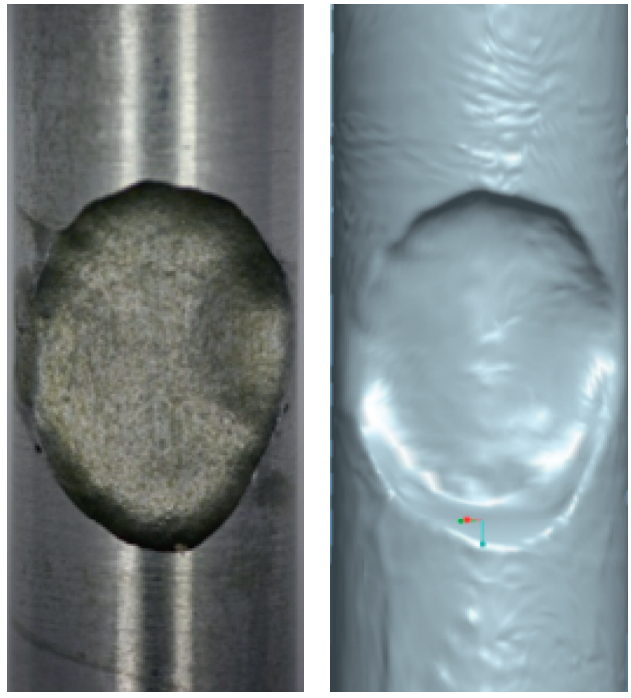

(a) (b)

Figure 4: Specimen FC3 and the reconstructed 3D surface model. (a) The actual specimen and the corrosion pit and (b) the reconstructed 3D surface model of the specimen using laser scanning data.

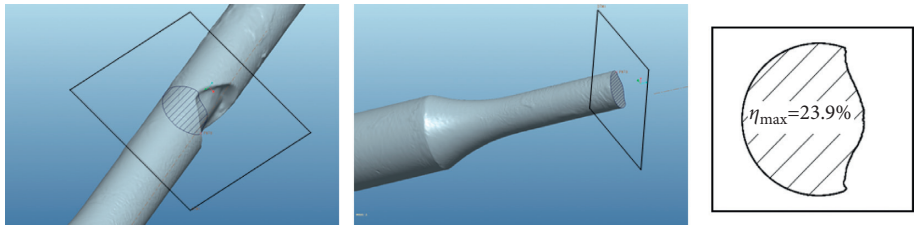

Figure 5: 3D surface profile measurements and pit geometry of the specimen FC3.

Table 3: Fatigue testing results of corroded specimens.

Specimen	Nominal stress range S (MPa)	MCD η_{max} (%)	Actual stress range σ (MPa)	Fatigue life N (cycle)
FC1	204.8	17.1	247.0	4060752
FC2	204.8	21.1	259.6	1415913
FC3	204.8	23.9	269.1	670622
FC4	204.8	30.1	293.0	338315
FC5	204.8	35.1	315.6	274103
FC6	286.7	19.6	356.6	99580
FC7	286.7	21.3	364.3	153070
FC8	286.7	21.6	365.7	201968
FC9	286.7	22.8	371.4	93330
FC10	286.7	29.8	408.4	35814
FC11	327.7	13.8	380.1	247064
FC12	327.7	14.6	383.7	348902
FC13	327.7	16.9	394.3	125903
FC14	327.7	23.8	430.0	27611

the parameters can trivially be obtained using the standard least square method; however, the deterministic fatigue life prediction makes little sense for practical applications due to the stochastic nature of fatigue process. To incorporate uncertainties, the probabilistic approach is usually preferred. In this study, the model parameters are identified statistically

Figure 6: Fatigue testing setup.

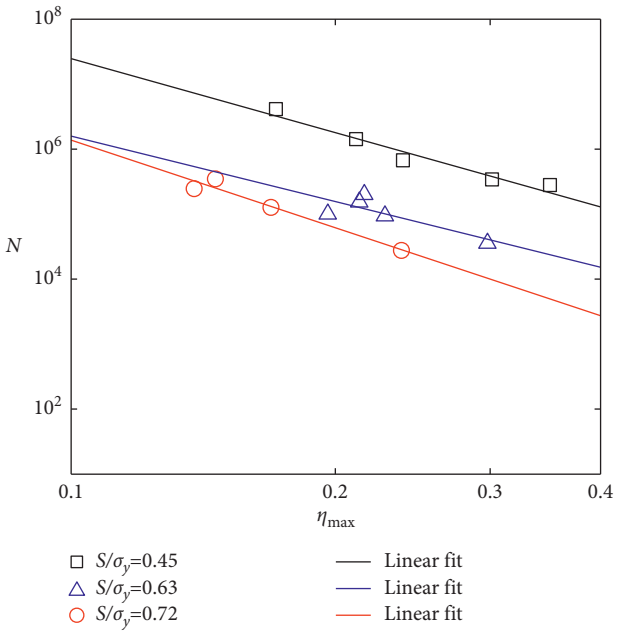

Figure 7: Relationship between fatigue life and MCD at three stress levels.

using the Bayesian estimator [29]. The core of the Bayesian method is to make inference based on prior information and data. The Bayesian posterior reads

$$p(\theta \mid D) \propto p(\theta) \cdot p(D \mid \theta), \tag{3}$$

where $p(\theta)$ is the prior probability density function (PDF) of a parameter (vector) θ, D is the data, $p(D \mid \theta)$ is the likelihood, and $p(\theta \mid D)$ is the posterior distribution. The posterior distribution of parameters θ can be asymptotically obtained using sampling methods, such as Markov chain Monte Carlo

(MCMC) simulation and its variants [30, 31]. Direct applications of the Bayesian method include parameter estimation and model updating. Without loss of generality, the model prediction error can be modeled as a zero-mean Gaussian variable. Based on this general assumption, the Bayesian estimator for the model parameters can be expressed as follows [32]:

$$p(A_1, A_2, A_3, \sigma_e) \propto \frac{1}{\sigma_e(\sqrt{2\pi}\,\sigma_e)^n} \exp\left\{-\frac{1}{2}\sum_{i=1}^{n}\left[\frac{\ln N - A_1 - A_2 \ln(S/\sigma_y) - A_3 \ln \eta_{\max}}{\sigma_e}\right]^2\right\}, \quad (4)$$

where σ_e is the standard deviation of the error variable, n is the number of available measurements, and $p(A_1, A_2, A_3, \sigma_e)$ is the posterior joint PDF. Using the experimental data of the specimens given in Table 3, 200,000 samples are drawn using MCMC simulations. The resulting distributions of model parameters A_1, A_2, A_3 and the standard deviation σ_e of the error variable are shown in Figure 8.

The model parameter vector (A_1, A_2, A_3) follows a multivariate normal distribution. The mean vector μ and the variance-covariance matrix Σ of the parameter vector (A_1, A_2, A_3) can be estimated from the MCMC samples as follows:

$$\mu = [\,2.4301 \quad -7.0829 \quad -3.9423\,], \quad (5)$$

$$\Sigma = \begin{bmatrix} 0.6601 & 0.3198 & 0.3108 \\ 0.3198 & 0.2857 & 0.1071 \\ 0.3108 & 0.1071 & 0.1643 \end{bmatrix}, \quad (6)$$

respectively. The standard deviation of the error variable σ_e follows a Gamma distribution with a shape parameter of 17.82 and a scale parameter of 0.0195. Using the mean of parameter vector (A_1, A_2, A_3), the mean prediction of the model is obtained as follows:

$$\ln N = 2.4301 - 7.0829 \ln\left(\frac{S}{\sigma_y}\right) - 3.9423 \ln \eta_{\max}. \quad (7)$$

To verify the effectiveness of the proposed model, the results of the mean prediction and the actual fatigue life are visually compared in Figure 9. A good agreement between model predictions (N_{pre}) and experimental data (N_{exp}) can be observed. The model with the prior distribution of (A_1, A_2, A_3) is used as the baseline model for Bayesian updating.

4. Bayesian Updating for General Applications

The baseline model above is constructed using data of the standard specimens. The dimension and size of the specimen can be quite different from those of a realistic corroded reinforcing bar in service [33]. Uncertain factors, such as residual stress introduced by the machining process of a component and the inherent dimensional deviations due to imperfect manufacturing, are difficult to quantify accurately without enough information [34–36]. To make the model more reliable, a scientific calibration of the model must be made. Bayesian updating is a rational way to incorporate new data into a baseline model. By performing the updating, the model is gradually calibrated to favor data of the actual component more than the prior state of knowledge [37].

To demonstrate the above idea and validate the effectiveness of method, Bayesian updating is performed using data reported in [13]. In that study, corroded steel reinforcing bars with two different diameters (10 mm and 12 mm) are extracted from reinforced concrete beams exposed to different corrosion degrees. The corrosion degrees are measured using the mass loss ratio ranging from 8% to 28%. Sinusoidal fatigue loads with nominal stresses of 150 MPa, 200 Mpa, and 300 MPa are applied at the frequency of 15 Hz. The details of the testing can be referred to in [13]. It should be noted that the corrosion damage in [13] is measured using the mass loss ratio. To utilize the proposed model, the formulation provided in [35] is used to transfer the mass loss ratio to MCD and is given as

$$\frac{A_{\min}}{A_{\text{ave}}} = 1 - 0.83\gamma, \quad (8)$$

where γ is the mass loss ratio, $A_{\min}$ is the minimum cross-sectional area, and A_{ave} is the averaged reduced cross-sectional area expressed as

$$A_{\text{ave}} = A_0(1 - \gamma). \quad (9)$$

The term A_0 is the uncorroded section area defined as before. Combining equations (1), (8), and (9), the MCD is established as follows:

$$\eta_{\max} = 1 - (1 - \gamma)(1 - 0.83\gamma). \quad (10)$$

Figure 10 presents the fatigue life prediction N_{pre} by the prior baseline model and the actual fatigue life data N_{exp} of the corroded steel reinforcing bars. The vertical bar of each prediction point represents 95% confidence intervals. The dashed lines and dot-dashed lines are the boundaries deviating from the actual fatigue life by the multiplication factors of 2 and 5, respectively. For example, given an x-coordinate value of N_{exp}, the values for the corresponding life factor 2 and life factor 5 are $2N_{\text{exp}}$ and $5N_{\text{exp}}$ in the y-coordinate. The overall trends of the model prediction agree with the experimental data, but the deviation of the prediction can be larger than a factor of 5. This means that the proposed model can capture the influence of stress range and MCD, but the direct application of the baseline

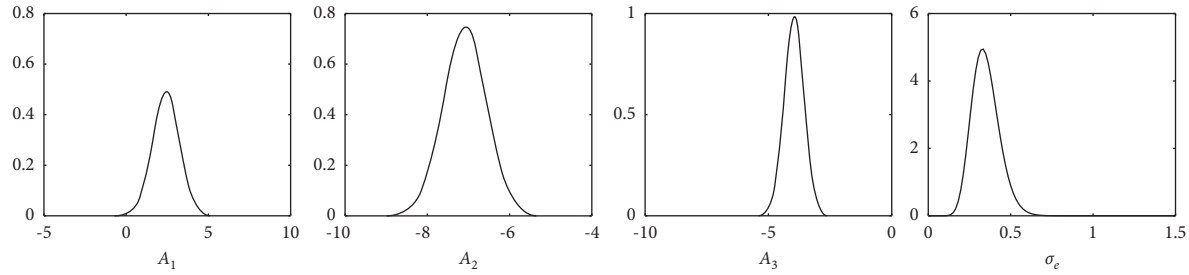

Figure 8: Distributions of A_1, A_2, A_3, and σ_e obtained using experimental data of standard specimens.

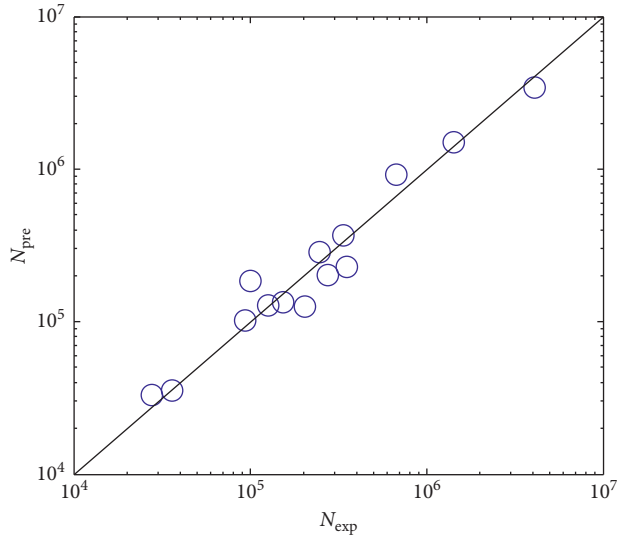

Figure 9: The experimental fatigue lives and model predictions.

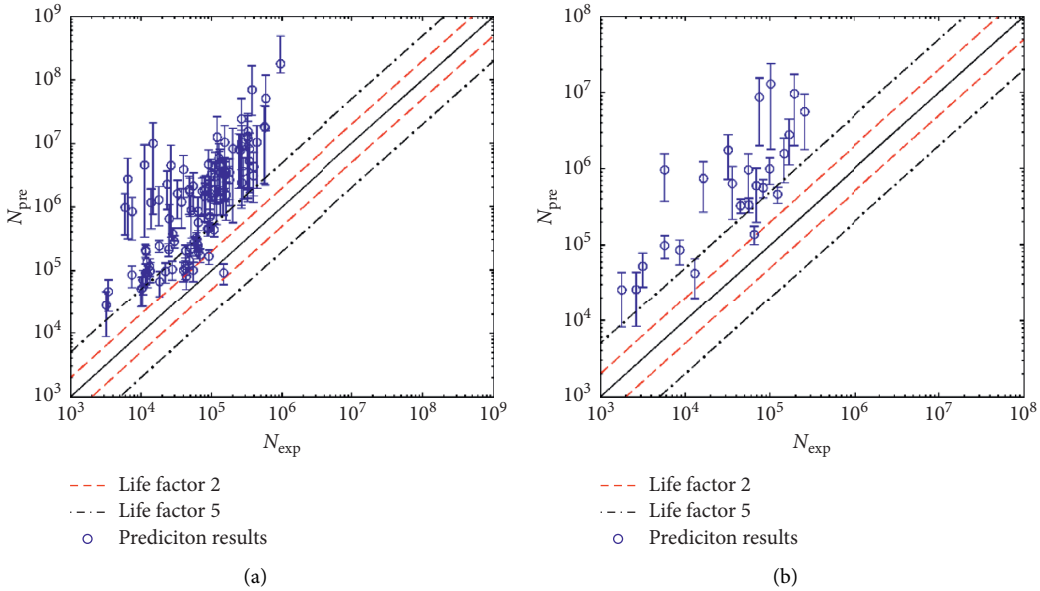

Figure 10: Fatigue life prediction results of the prior mean model in equation (7). (a) Steel bars with diameter of 12 mm and (b) steel bars with diameter of 10 mm.

Table 4: Testing results (12 mm-diameter bars) arbitrarily chosen from [13], representing observed data for Bayesian updating.

No.	Nominal stress range S (MPa)	MCD $\eta_{\max}$ (%)	Fatigue life N (cycle)
1	200	34.2	5909
2	300	29.2	27798
3	300	23.4	63818
4	200	24.9	99873
5	300	30.7	12353
6	300	26.8	48224
7	200	30.9	79579
8	200	22.4	343394
9	200	35.5	7485
10	200	38.0	25064
11	200	30.1	32852
12	300	29.5	54870
13	300	23.0	62138
14	300	25.9	92051
15	200	19.5	264010
16	150	15.3	943043

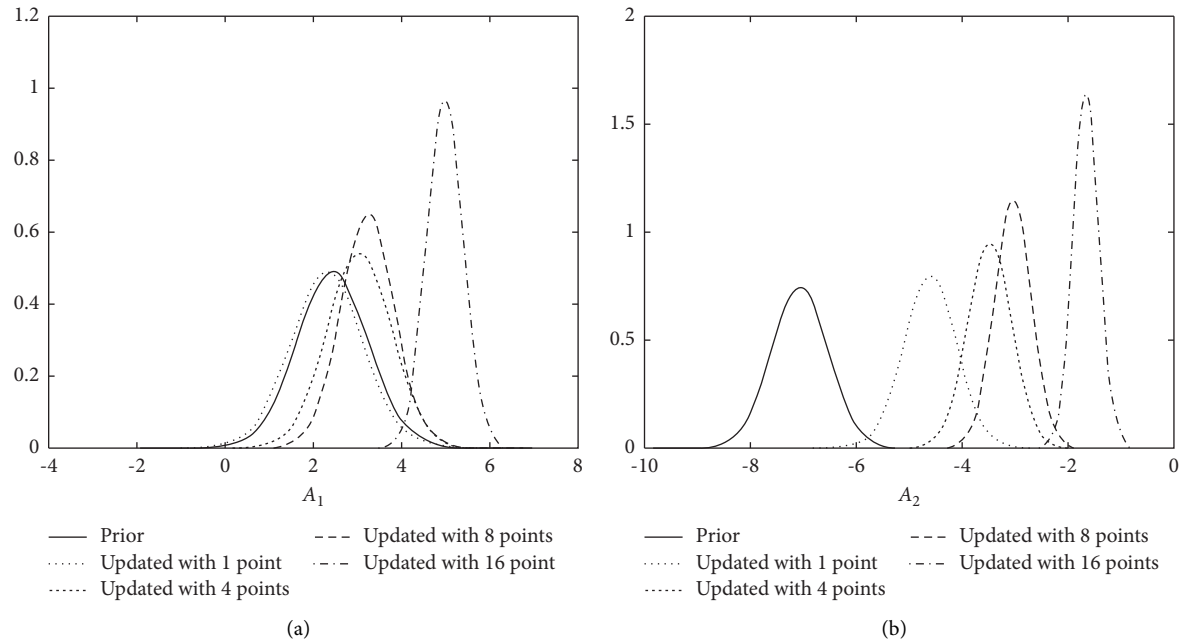

(a) (b)

Figure 11: Continued.

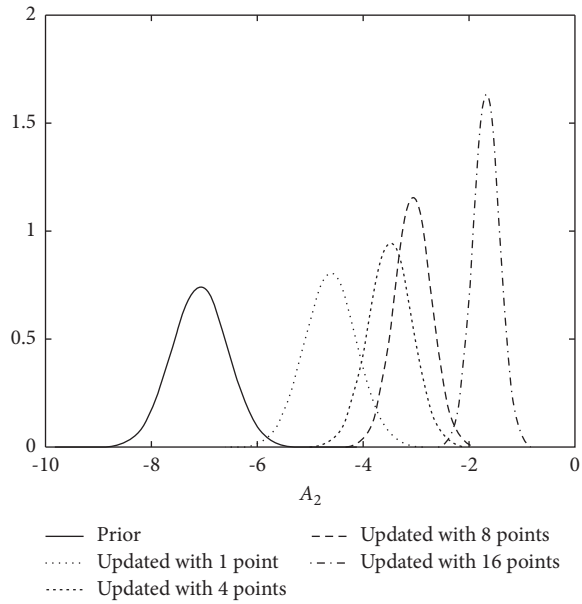

(c)

Figure 11: The prior and posterior distributions of model parameters (diameter: 12 mm). (a) Parameter A_1, (b) parameter A_2, and (c) parameter A_3.

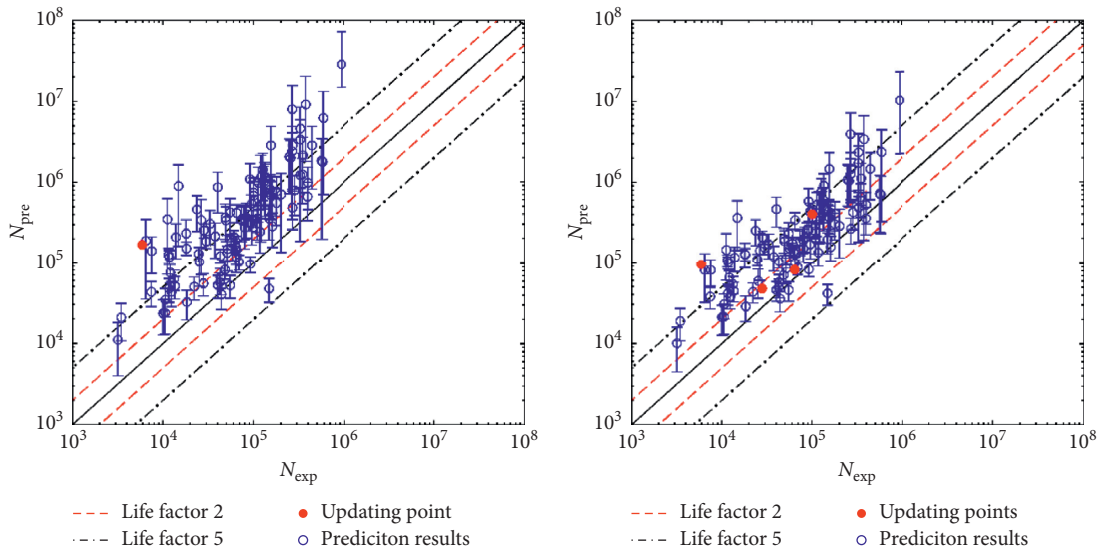

(a) (b)

Figure 12: Continued.

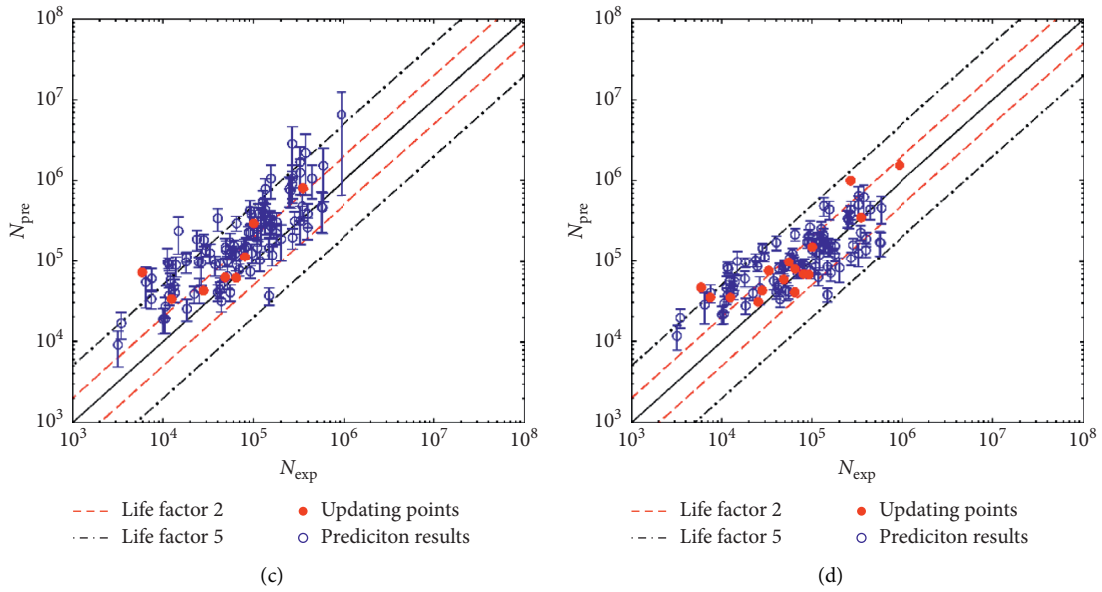

Figure 12: Fatigue life prediction results for 12 mm-diameter bars using the model updated with (a) 1 point, (b) 4 points, (c) 8 points, and (d) 16 points.

Table 5: Testing results (10 mm-diameter bars) arbitrarily chosen from [13], representing observed data for Bayesian updating.

No.	Nominal stress range S (MPa)	MCD η_{max} (%)	Fatigue life N (cycle)
1	300	40.8	1785
2	300	30.1	8603
3	200	37.4	35988
4	300	18.6	82951
5	200	33.7	5706
6	200	35.9	16346
7	300	21.3	55970
8	300	19.6	122934
9	300	29.0	5715
10	300	34.0	3157
11	300	35.9	12959
12	200	29.0	31959
13	300	21.4	44883
14	200	38.0	68812
15	200	17.5	102030
16	200	18.8	192984

model of equation (7) is not reliable due to the uncertainties between the specimens and the real components.

The actual data of the bars are used for Bayesian updating. The posterior PDF of the model parameters writes

$$p(A_1, A_2, A_3|D) \propto \frac{1}{2\pi\sqrt{|\Sigma|}} \exp\left[-\frac{1}{2}\left([A_1, A_2, A_3] - \mu\right)\Sigma^{-1}\left([A_1, A_2, A_3] - \mu\right)^{\mathrm{T}}\right] \times \frac{1}{\left(\sqrt{2\pi}\,\sigma_e\right)^n} \exp\left\{-\frac{1}{2}\sum_{i=1}^{n}\left[\frac{\ln N - A_1 - A_2 \ln\left(S/f_y\right) - A_3 \ln \eta_{max}}{\sigma_e}\right]\right\}, \tag{11}$$

where the mean vector μ and the covariance matrix Σ are given by equations (5) and (6), respectively. The mean value of σ_e is estimated as 0.34 from the prior distribution and is used in equation (11).

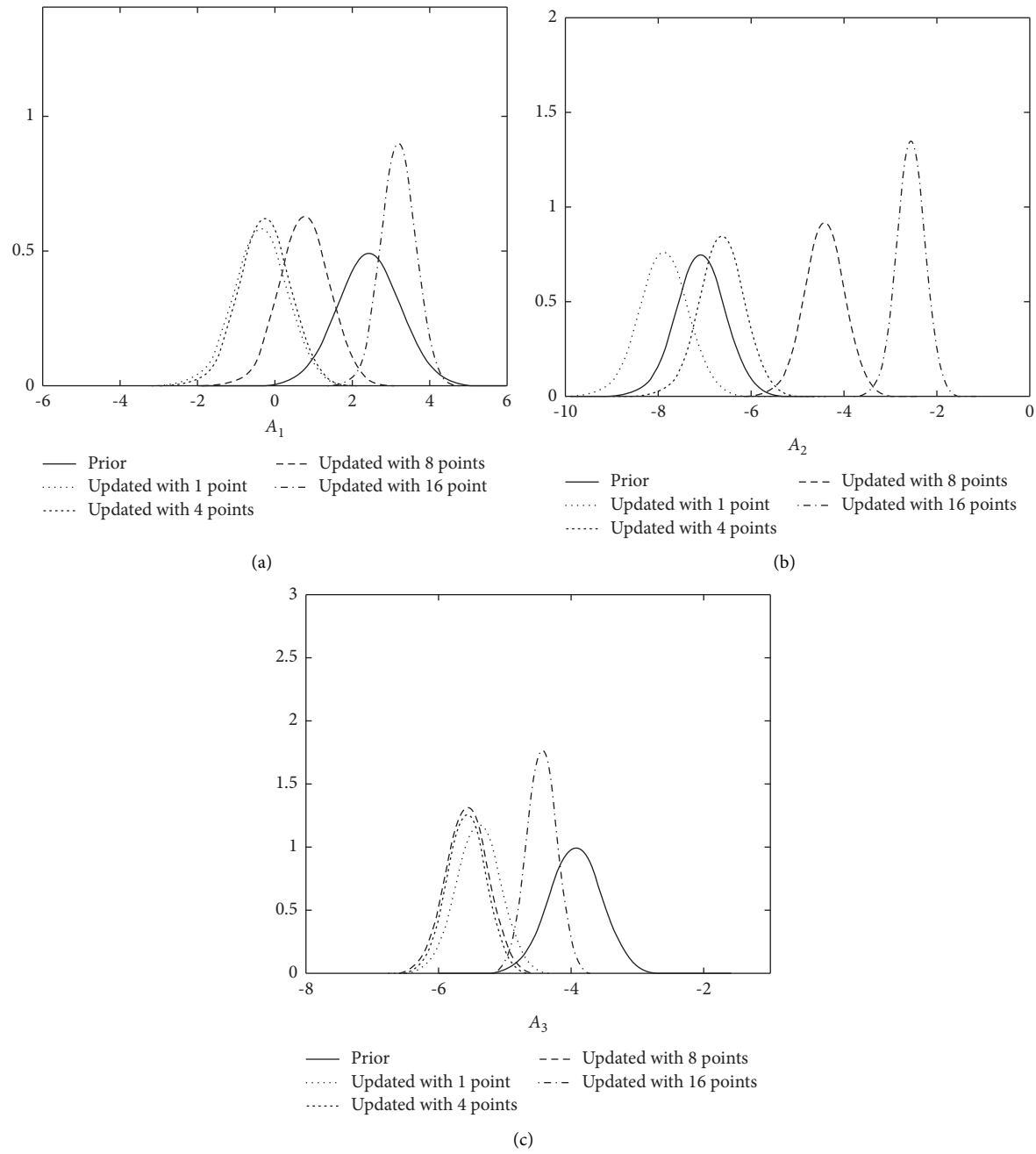

FIGURE 13: The prior and posterior distributions of model parameters (diameter: 10 mm). (a) Parameter A_1, (b) parameter A_2, and (c) parameter A_3.

4.1. Case 1—Steel Bars with a Diameter of 12 mm. A total number of 16 specimens are arbitrarily chosen from [13] to represent the observation data for Bayesian updating, and they are denoted as updating points. The total 16 sets of (S, $\eta_{\max}$, N) are listed in Table 4 and are used in the posterior of equation (11). The posterior results updated with 1, 4, 8, and 16 data points in Table 4 are evaluated using MCMC simulations. For each of the four updates, 200,000 samples are drawn, and the samples are used to estimate the PDFs of the model parameter vector (A_1, A_2, A_3). The prior and posterior distributions of the model parameters A_1, A_2, and A_3 are presented in Figures 11(a)–11(c), respectively. As more data are used for updating, the distributions are gradually tuned to be more specific to the actual components.

The fatigue life prediction results of the specimens in [13] other than those used for updating are obtained using the resulting MCMC samples and equation (7). The calculation procedure is as follows. For each of the specimens, that is, the discrete hollow points in Figure 12, the stress (S) and MCD ($\eta_{\max}$) associated with the specimen, and a random instance of the resulting MCMC samples is used in equation (7) to compute one sample of the fatigue life N_{pre}. By using a total number of 200,000 random instances, a total number of

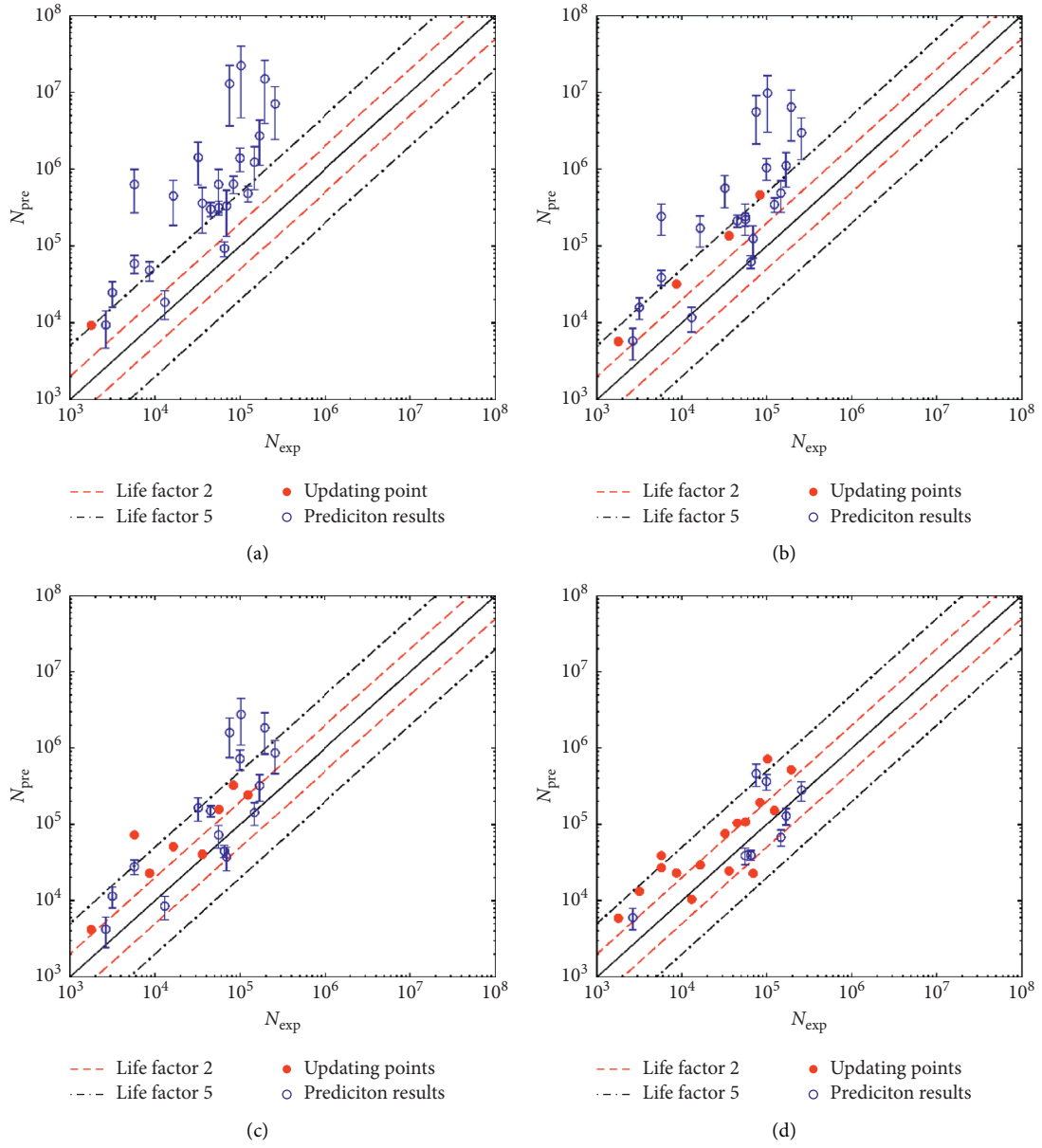

Figure 14: Fatigue life prediction results for 10 mm-diameter bars using the model updated with (a) 1 point, (b) 4 points, (c) 8 points, and (d) 16 points.

200,000 random samples of the fatigue life of the specimen are evaluated, and the mean and 95% confidence bounds are estimated from the fatigue life samples. Figure 12 presents the prediction results of the updated model with 1, 4, 8, and 16 updating points. The red solid points are the data used for updating and the blue hollow points are prediction results of the rest of the specimens in the dataset. The vertical bar of each prediction point represents 95% confidence intervals. It can be observed from Figure 12 that the fatigue life predictions gradually converge to the experimental results as more and more data are used for updating. It indicates that as more and more relevant information is integrated into the model through Bayesian updating, the features of the realistic reinforcing bars tend to dominate the posterior, yielding more accurate prediction results.

4.2. Case 2—Steel Bars with a Diameter of 10 mm. The same Bayesian updating procedure is performed for the steel bars with a diameter of 10 mm. A total number of 16 sets of testing results on the 10 mm-diameter bar are arbitrarily chosen from [13] to represent the actually observed data presented in Table 5, which are used for Bayesian updating. Figures 13(a)–13(c) present the posterior distributions of model parameters A_1, A_2, and A_3, respectively, updated with 1, 4, 8, and 16 points in Table 5 using the posterior of equation (11). The prediction results of the updated model are shown in Figure 14. It can be seen that the updated model yields more and more accurate results as more data are incorporated into the baseline model.

The above two cases demonstrate that the initial baseline model cannot yield accurate results due to the

deviation between the two sets of specimens under fatigue testing. However, as more observation data are incorporated into the baseline model via Bayesian updating, the predictions results can be largely improved. In particular, when the baseline model is updated with 16 data points, most of the life prediction results shown in Figures 12(d) and 14(d) are within the bounds deviated from the actual life by a factor of 5. The updated model with 16 data points has the ability to estimate the fatigue life in different corrosion specimens.

5. Conclusion

This paper proposes a general method for fatigue life prediction of corroded reinforcing bars using testing data of standard specimens and Bayesian updating. To investigate the influencing factors of the fatigue life, a systematical fatigue testing is performed. The local geometry details of the corrosion pits are acquired using the advanced 3D laser scanning technique. Based on 3D measurements of the corrosion pits and fatigue life data, the maximum corrosion degree and stress range are found to be effective in characterizing the fatigue life. A fatigue life model is proposed incorporating the two factors. The parameters of the model are statistically obtained using the testing data, and the resulting model is used as a baseline model for general applications. Due to the variations of the dimension and working condition of an actual reinforcing bar, the Bayesian method is used to update the baseline model using data from the actual reinforcing bars. The proposed method is demonstrated using independent fatigue testing data of steel reinforcing bars. Based on the current results, the following conclusions are drawn:

(1) The normalized nominal stress range and maximum corrosion degree are effective factors to quantify the fatigue life of corroded steel reinforcing bars. Experimental data show that the fatigue life has a log-linear relationship with the maximum corrosion degree under different stress ranges. A regression model incorporating the two factors can be used to characterize the fatigue life of corroded reinforcing bars.

(2) The proposed baseline model can be applied to more general applications where the dimension and working condition of a reinforcing bar differ from that of the standard specimen. This is achieved by updating the initial model using the Bayesian method. The effectiveness of the method is demonstrated using reinforcing bars with different diameters under different fatigue loads.

(3) The model obtained from Bayesian updating with 16 data points is observed to have the ability to predict the fatigue life of different specimens accurately. It is shown that most of the prediction results are within the bounds deviated from the actual life by a factor of 5.

It is worth mentioning that the corrosion-free fatigue testing results are indispensable as a reference for comparison purposes. Due to the time and resource limitations on the current study, the corrosion-free fatigue testing will be performed in the future study.

Data Availability

The data included in this study are generated by the authors during the study.

Disclosure

The work was done when J. Chen was at School of Transportation Science and Engineering, Beihang University, 37 Xueyuan Rd., Beijing 100191, China.

Conflicts of Interest

The authors declare that they have no conflicts of interest.

Acknowledgments

This work was supported by the National Natural Science Foundation of China (nos. 51678021 and U1930403). The support is greatly acknowledged.

References

[1] C. Gehlen, K. Osterminski, and T. Weirich, "High-cycle fatigue behaviour of reinforcing steel under the effect of ongoing corrosion," *Structural Concrete*, vol. 17, no. 3, pp. 329–337, 2016.

[2] Z. J. Liu, B. Diao, and X. N. Zheng, "Effects of seawater corrosion and freeze-thaw cycles on mechanical properties of fatigue damaged reinforced concrete beams," *Annals of Materials Science & Engineering*, vol. 2015, pp. 15–30, 2015.

[3] W. J. Yi, S. K. Kunnath, X. D. Sun, C. J. Shi, and F. J. Tang, "Fatigue behavior of reinforced concrete beams with corroded steel reinforcement," *ACI Structural Journal*, vol. 107, no. 5, pp. 526–533, 2010.

[4] Y. Ma, Z. Guo, L. Wang, and J. Zhang, "Probabilistic life prediction for reinforced concrete structures subjected to seasonal corrosion-fatigue damage," *Journal of Structural Engineering*, vol. 146, no. 7, Article ID 04020117, 2020.

[5] Z. Guo, Y. Ma, L. Wang, J. Zhang, and I. E. Harik, "Corrosion fatigue crack propagation mechanism of high-strength steel bar in various environments," *Journal of Materials in Civil Engineering*, vol. 32, no. 6, Article ID 04020115, 2020.

[6] J. He, H. Huo, X. Guan, and J. Yang, "A Lamb wave quantification model for inclined cracks with experimental validation," *Chinese Journal of Aeronautics*, vol. 34, no. 2, pp. 601–611, 2021.

[7] X. Wang, Y. Zhao, L. Wang, L. Wei, J. He, and X. Guan, "In-situ SEM investigation and modeling of small crack growth behavior of additively manufactured titanium alloy," *International Journal of Fatigue*, vol. 149, Article ID 106303, 2021.

[8] A. Salaheldin and J. Lovegrove, "Fatigue of cold worked ribbed reinforcing bar-a fracture mechanics approach," *International Journal of Fatigue*, vol. 4, no. 1, pp. 15–26, 1982.

[9] T. Makita and E. Brühwiler, "Tensile fatigue behaviour of ultra-high performance fibre reinforced concrete combined

with steel rebars (R-UHPFRC)," *International Journal of Fatigue*, vol. 59, pp. 145–152, 2014.

[10] R. A. Hawileh, J. A. Abdalla, A. Al Tamimi, K. Abdelrahman, and F. Oudah, "Behavior of corroded steel reinforcing bars under monotonic and cyclic loadings," *Mechanics of Advanced Materials and Structures*, vol. 18, no. 3, pp. 218–224, 2011.

[11] A. A. Almusallam, "Effect of degree of corrosion on the properties of reinforcing steel bars," *Construction and Building Materials*, vol. 15, no. 8, pp. 361–368, 2001.

[12] B. El Hajj, F. Schoefs, B. Castanier, and T. Yeung, "A condition-based deterioration model for the stochastic dependency of corrosion rate and crack propagation in corroded concrete structures," *Computer-Aided Civil and Infrastructure Engineering*, vol. 32, no. 1, pp. 18–33, 2017.

[13] I. Fernandez, J. M. Bairán, and A. R. Marí, "Corrosion effects on the mechanical properties of reinforcing steel bars. Fatigue and σ-ε behavior," *Construction and Building Materials*, vol. 101, pp. 772–783, 2015.

[14] M. B. Anoop, B. K. Raghuprasad, and K. Balaji Rao, "A refined methodology for durability-based service life estimation of reinforced concrete structural elements considering fuzzy and random uncertainties," *Computer-Aided Civil and Infrastructure Engineering*, vol. 27, no. 3, pp. 170–186, 2012.

[15] H. W. Tang, S. B. Li, D. H. Xie, and C. Zhu, "Research on fatigue S-N curves of corrosion-damaged reinforcement," *Key Engineering Materials*, vol. 324-325, pp. 607–610, 2006.

[16] S. Li, W. Zhang, X. Gu, and C. Zhu, "Fatigue of reinforcing steel bars subjected to natural corrosion," *The Open Civil Engineering Journal*, vol. 5, pp. 69–74, 2011.

[17] Y. Ma, Q. Wang, Z. Guo, G. Wang, L. Wang, and J. Zhang, "Static and fatigue behavior investigation of artificial notched steel reinforcement," *Materials*, vol. 10, no. 5, 2017.

[18] W. Zhang, X. Song, X. Gu, and S. Li, "Tensile and fatigue behavior of corroded rebars," *Construction and Building Materials*, vol. 34, pp. 409–417, 2012.

[19] Y. Huang, X. Ye, B. Hu, and L. Chen, "Equivalent crack size model for pre-corrosion fatigue life prediction of aluminum alloy 7075-T6," *International Journal of Fatigue*, vol. 88, pp. 217–226, 2016.

[20] M. Cerit, K. Genel, and S. Eksi, "Numerical investigation on stress concentration of corrosion pit," *Engineering Failure Analysis*, vol. 16, no. 7, pp. 2467–2472, 2009.

[21] K. Andisheh, A. Scott, and A. Palermo, "Modeling the influence of pitting corrosion on the mechanical properties of steel reinforcement," *Materials and Corrosion*, vol. 67, no. 11, pp. 1220–1234, 2016.

[22] in*General Administration of Quality Supervision Inspection and Quarantine of the People's Republic of China, Metallic Materials - Tensile Testing - Part 1: Method of Test at Room Temperature*Beijing, ChinaGB/T228.1–2010, 2010.

[23] in*General Administration of Quality Supervision Inspection and Quarantine of the People's Republic of China, Metallic Materials - Fatigue Testing - Axial-Force-Controlled Method*Beijing, China*GB/T 3075-2008*, 2008.

[24] F. Tang, Z. Lin, G. Chen, and W. Yi, "Three-dimensional corrosion pit measurement and statistical mechanical degradation analysis of deformed steel bars subjected to accelerated corrosion," *Construction and Building Materials*, vol. 70, pp. 104–117, 2014.

[25] F. Qi, N. Chen, and Q. Wang, "Preparation of PA11/BaTiO3 nanocomposite powders with improved processability, dielectric and piezoelectric properties for use in selective laser sintering," *Materials & Design*, vol. 131, pp. 135–143, 2017.

[26] K. C. Aw, W. D. J. Huang, and M. W. R. P. De Silva, "Evaluation of climatic vibration testing on plastic waterproof enclosure for electronic equipment using ANSYS workbench," *Materials & Design*, vol. 28, no. 9, pp. 2505–2510, 2007.

[27] R. Zhang and S. Mahadevan, "Model uncertainty and Bayesian updating in reliability-based inspection," *Structural Safety*, vol. 22, no. 2, pp. 145–160, 2000.

[28] C. Gao, Z. Fang, J. Lin, X. Guan, and J. He, "Model averaging and probability of detection estimation under hierarchical uncertainties for Lamb wave detection," *Mechanical Systems and Signal Processing*, vol. 165, Article ID 108302, 2022.

[29] D. Zhou, J. He, Y.-M. Du, C. P. Sun, and X. Guan, "Probabilistic information fusion with point, moment and interval data in reliability assessment," *Reliability Engineering & System Safety*, vol. 213, Article ID 107790, 2021.

[30] W. K. Hastings, "Monte Carlo sampling methods using Markov chains and their applications," *Biometrika*, vol. 57, no. 1, pp. 97–109, 1970.

[31] D. Zhou, C. P. Sun, Y.-M. Du, and X. Guan, "Degradation and reliability of multi-function systems using the hazard rate matrix and Markovian approximation," *Reliability Engineering & System Safety*, vol. 218, Article ID 108166, 2022.

[32] J. He, W. Wang, M. Huang, S. Wang, and X. Guan, "Bayesian inference under small sample sizes using general noninformative priors," *Mathematics*, vol. 9, no. 21, p. 2810, 2021.

[33] Y.-C. Ou, Y. T. T. Susanto, and H. Roh, "Tensile behavior of naturally and artificially corroded steel bars," *Construction and Building Materials*, vol. 103, pp. 93–104, 2016.

[34] G. P. Tilly, "Fatigue testing and performance of steel reinforcement bars," *Matériaux et Constructions*, vol. 17, no. 1, pp. 43–49, 1984.

[35] M. M. Kashani, A. J. Crewe, and N. A. Alexander, "Use of a 3D optical measurement technique for stochastic corrosion pattern analysis of reinforcing bars subjected to accelerated corrosion," *Corrosion Science*, vol. 73, no. 13, pp. 208–221, 2013.

[36] J. He, M. Huang, W. Wang, S. Wang, and X. Guan, "An asymptotic stochastic response surface approach to reliability assessment under multi-source heterogeneous uncertainties," *Reliability Engineering & System Safety*, vol. 215, Article ID 107804, 2021.

[37] M. Mishra, J. Martinsson, K. Goebel, and M. Rantatalo, "Bearing life prediction with informed hyper-prior distribution: a Bayesian hierarchical approach," *IEEE/ASME transactions on mechatronics*, vol. 9, pp. 157002–157011, 2018.